Physica D 60 (1992) 112–138
North-Holland

PHYSICA D

High order finite volume approximations of differential operators on nonuniform grids *

James M. Hyman [a], Robert J. Knapp [c] and James C. Scovel [b]

[a] *Theoretical Division, MS B284, Center for Nonlinear Studies, Los Alamos National Laboratory, Los Alamos, NM 87545, USA*

[b] *Computing Division, MS B265, Center for Nonlinear Studies, Los Alamos National Laboratory, Los Alamos, NM 87545, USA*

[c] *Department of Mathematics, Bowdoin College, Brunswick, ME 04011, USA*

When computing numerical solutions to partial differential equations, difference operators that mimic the crucial properties of the differential operators are usually more accurate than those that do not. Properties such as symmetry, conservation, stability, and the duality relationships and identities between the gradient, curl, and divergence operators are all important. Using the finite volume method, we have derived local, accurate, reliable and efficient difference methods that mimic these properties on nonuniform rectangular and cuboid grids. In a finite volume method, the divergence, gradient, and curl operators are defined using a discrete versions of the divergence theorem and Stokes' theorem. These methods are especially powerful on coarse nonuniform grids and in calculations where the mesh moves to track interfaces or shocks. Numerical examples comparing local second and fourth-order finite volume approximations to conservation laws on very rough grids are used to demonstrate the advantages of the higher order methods.

1. Introduction

When computing numerical solutions to partial differential equations (PDEs), difference operators that mimic the crucial properties of the differential operators are usually more accurate than those that do not. Properties such as symmetry, conservation, stability, and the duality relationships and identities between the gradient, curl, and divergence are all important. In this paper we will concentrate on local, accurate, reliable and efficient difference methods that mimic these properties. These mimetic difference schemes will be derived using the finite volume method.

In this paper we distinguish difference schemes by the methodology used to derive them. In *finite difference methods* (FDM) [9], the discrete approximations to differential operators are derived by interpolating (e.g., Lagrange or least-squares polynomial, splines, trigonometric function) pointwise values of a function defined on a discrete mesh and differentiating the interpolant to obtain approximations of the derivatives. In most of the FDMs, the derivative approximations are explicit linear combinations of the neighboring function values.

In a *finite element method* (FEM) [13] the function defined on the mesh is assumed to satisfy the variational form of some differential equation. The solution to this equation is approximated by

* Work performed under the auspices of the US Department of Energy under contract W-7405-ENG-36 and the Applied Mathematical Sciences contract KC-07-01-01.

Elsevier Science Publishers B.V.

restricting both the function and its variations to lie in the linear span of a finite number of basis functions. Galerkin's method generalizes the FEM to nonvariational settings. Approximations of a differential operator can be extracted analytically by differentiating the basis functions.

In a *finite volume method* (FVM) [16] the average values of a function over local mesh cells are taken as the unknowns. Discrete approximations of the divergence, gradient, and curl operators are defined using general forms of Stokes' Theorem; and the scalar Laplacian is computed as the divergence of the gradient.

The resulting formulas for these three methods are very often identical on uniform grids but can differ greatly in irregular grids. The FDMs are usually local (in the sense that they are explicit linear combinations of the nearby function values) and accurate but, on irregular grids, they may lose the stability and symmetry properties of the differential operator they are approximating. The FEMs are nonlocal, accurate and preserve these properties even on irregular grids. The FEMs can be "lumped" [13] to give formulas that are local, but the derivative approximations given by the local lumped formulas are often inaccurate. The FVMs are local, accurate and preserve the stability and symmetry properties of the differential operators. One of the goals of this paper is to define a methodology to derive high order accurate FVMs on irregular grids.

FDMs are commonly available to accurately approximate differential operators on uniform grids [1–4,9]. In particular, approximations to the divergence and gradient operators are available to arbitrary order by locally interpolating the function values with a Lagrange interpolating polynomial. Most of the discrete approximations on uniform grids mimic the stability and symmetries of the differential operators; this is rarely the case on nonuniform grids. These discrepancies can often be overcome by using a nonlocal difference formulation such as the FEM. Unfortunately, this requires solving a large algebraic system of equations to obtain accurate derivative approximations. Also, the entire grid configuration needed to apply a nonlocal method may not always be available at each stage of a calculation. This is often the case in methods based on domain decomposition or when solving problems on parallel computers with distributed memory.

Because the FVM uses Stokes' theorem to obtain its formulas approximating the differential operators, they automatically satisfy a discrete Stokes' theorem. For definiteness, consider three dimensions, for which we introduce the identifications: for point and cell volume quantities ω is a scalar and in the former case, $d\omega = \nabla\omega$. For line segment and cell face quantities, ω is a vector and $d\omega = \nabla \times \omega$ [10]. The approach may be used for any differential operation corresponding to the exterior derivative. For example, in three dimensions, the exterior derivatives correspond to divergence, gradient and curl. Stokes' theorem $\int_\Omega d\omega = \int_{\partial\Omega} \omega$ is the defining relation for these operations.

We shall be applying the FVMs to approximate partial differential equations (PDEs) in their locally integrated form. That is, the spatial domain of interest will have been cut up into a set of nonoverlapping finite volume cells, and we shall be approximately solving for the local integral of the solution over each of these cells. The solution of the PDE satisfies certain relationships between the change in its average value over a cell and boundary integrals around the cell. These relationships hold not only for each cell but also for the union of cells. They also hold for the FVM solution's local integrals because of the underlying integral equation and because the local boundary integrals of the solution are defined consistently and (except for sign) independently of the side of the boundary one is considering (the sign alters in a fashion consistent with the side of the boundary under consideration.). Hence, when using the FVM, the analogs of appropriate integral identities are satisfied over unions of cells automatically because of a telescoping cancelation that occurs when the local boundary integral terms are summed to calculate the total contributions over the union of cells. Thus, for FVMs, the

corresponding analogs of integral identities hold for arbitrary unions of the cells, independent of how accurate or inaccurate the approximation is.

In section 2, we rewrite the divergence theorem and (the usual) Stokes' theorem as relations between the mean value of quantities over local volumes, faces, edges (whatever seems most appropriate) in such a way that the integrals over the unions of local regions would be written as the sum of the integrals over local regions (with the requirement that shared boundaries between cells have oppositely directed boundary integrals when considering the two adjacent cells). Thus, in this section we construct mnemonics that will be used to keep track of quantities whose further definition, we shall insist, must be handled consistently, from spatial cell to cell, in order to insure appropriate cancellation upon taking unions of cells.

Sections 3 and 4 describe additional relations to improve the accuracy of FVMs. In selecting the unknown quanities to use with the FVM, we have chosen the mean-value of the solution over a cell to be the primary unknown. We make this choice because it is the integral over spatial regions that is "conserved" in conservation laws, and because this is the item of prime importance in FVMs. Moreover, so that we have a minimal number of unknowns, we shall use nothing else but these cell mean-values as our independent variables. But as our local integral relationships from the PDE relate local volume integrals to local boundary integrals, we must express the boundary integrals (over faces, edges, and even point value of functions) in terms of the cell mean-values associated with nearby cells. As we shall see, the more neighboring mean-values used to relate the cell mean-values and the boundary integrals, the more accurate the FVM can be made. Indeed, the methods end up looking very like the higher order FDMs. But, unlike FDMs on nonuniform grids, the analogs of certain integral identities will automatically hold, because all will be done consistent with methodology derived in section 2 to insure consistency between the cell-face, cell-edge, and local point values of the approximate solution.

After the general overview of the FVM for one and two dimensional operators, we derive local FVM approximations for operators defined on irregular one- and two-dimensional logically rectangular grids and show, by numerical examples, the advantage of the higher order methods. In appendix A, we show that the recommended FVM approximation of the Laplacian is positive definite on tensor products of uniform grids (Δx not necessarily equal to Δy).

We had hoped to obtain nine point FVM formulas on logically rectangular grids that are exact for quadratic functions. However, we show in appendix B that, for a reasonably large class of distorted grids, the coefficients of the difference formulas for the gradient can become unbounded if we force the approximation to be exact for arbitrary quadratic functions. Because of the close relationship between the gradient and the Laplacian, this result suggests that there may not exist a stable nine point, symmetric, positive definite, approximation to the Laplacian that is exact for quadratic scalar functions on all logically rectangular grids. For tensor product grids we do provide an accurate, symmetric nine point approximation to the Laplacian that is exact for quadratic functions.

2. Finite volume method

Many physically motivated systems of PDEs are derived from a limiting process applied to integral equations. For example, a quantity u is conserved under the flow of a conservation law if the amount of u contained in any fixed volume Ω is due entirely to the flux $f(u)$ across the boundary $\partial\Omega$ of Ω. These conservation laws can be expressed in integral form as

$$\frac{\mathrm{d}}{\mathrm{d}t}\int_{\Omega} u = \int_{\partial\Omega} \boldsymbol{f}(u)\cdot\hat{\boldsymbol{n}}, \tag{2.1}$$

where $\hat{\boldsymbol{n}}$ denotes the outward normal to the boundary.

Moving the time derivative under the integral sign and applying the divergence theorem, eq. (2.1) can be rewritten as

$$\int_{\Omega} [\partial_t u + \nabla\cdot\boldsymbol{f}(u)] = 0. \tag{2.2}$$

By letting the volume shrink to a point, we obtain the PDE

$$\partial_t u + \nabla\cdot\boldsymbol{f} = 0 \tag{2.3}$$

at every point where u and $\boldsymbol{f}$ are differentiable.

When numerically solving eq. (2.1) it is natural to stop the limiting process at the local mesh spacing and solve (2.2) where the control volumes Ω are the local mesh cells.

More precisely, in a small time-invariant, three-dimensional control volume, we write the integral relation (2.2) as $(\partial/\partial t)\overline{\overline{\overline{u}}} + \overline{\overline{\overline{\nabla\cdot\boldsymbol{f}}}} = 0$. Here the number of bars denote the number of dimensions averaged over (for example, $\overline{\overline{\overline{\cdot}}}$ represents a three dimensional cell average), and the divergence theorem is applied in computing $\overline{\overline{\overline{\nabla\cdot\boldsymbol{f}}}}$ by acting on face-averaged normal components of fluxes:

$$\overline{\overline{\overline{\nabla\cdot\boldsymbol{f}}}} := \frac{1}{\mathrm{Vol}(\Omega)}\int_{\Omega}\nabla\cdot\boldsymbol{f}\,\mathrm{d}\,\mathrm{Vol} = -\frac{1}{\mathrm{Vol}(\Omega)}\int_{\partial\Omega}\boldsymbol{f}\cdot\hat{\boldsymbol{n}} = -\frac{1}{\mathrm{Vol}(\Omega)}\sum_j A_j\overline{\overline{f}}_j. \tag{2.4}$$

Here the time independent control volume Ω is bordered by the mesh points, its boundary is the union of J distinct pieces, $\partial\Omega = \cup(\partial\Omega)_j$, $j = 1,\ldots,J$. Moreover, here A_j is the area of the jth piece, and $\overline{\overline{f}}_j$ may be interpreted as the normal component of $\boldsymbol{f}$ over the jth piece given by

$$\overline{\overline{f}}_j := \frac{1}{A_j}\int_{(\partial\Omega)_j}\boldsymbol{f}\cdot\hat{\boldsymbol{n}}. \tag{2.5}$$

The central idea behind the FVM is to accurately approximate $\overline{\overline{f}}_j$ and use (2.4) to define a discrete approximation of $\overline{\overline{\overline{\nabla\cdot\boldsymbol{f}}}}$.

The discrete curl of a vector field $\boldsymbol{v}$ is defined using Stokes' theorem. Instead of a cell volume quantity, this vector lives on two-dimensional cells S and can be defined by the following operator acting on edge-averaged tangential components of vectors:

$$\overline{\overline{\nabla\times\boldsymbol{v}}} := \frac{1}{\mathrm{Area}\ (\mathrm{S})}\int_{S}\nabla\times\boldsymbol{v}\cdot\hat{\boldsymbol{n}} = \frac{1}{\mathrm{Area}\,(\mathrm{S})}\int_{\partial S}\boldsymbol{v}\cdot\mathrm{d}\boldsymbol{r} = \frac{1}{\mathrm{Area}\,(\mathrm{S})}\sum_j l_j\overline{v}_j, \tag{2.6}$$

where ∂S has boundary components $\partial S = (\partial S)_j$, and $\overline{v}_j = (1/l_j)\int_{(\partial S)_j}\boldsymbol{v}\cdot\mathrm{d}\boldsymbol{r}$ is the integral of the tangential components of $\boldsymbol{v}$ over the jth piece of the boundary with length l_j.

Similarly, the discrete gradient of a function is a line segment quantity: if ℓ is a line segment, the discrete gradient operator acts on point values at the end of the segment. That is,

$$\overline{\nabla f} := \frac{1}{\text{length }(\ell)} \int_{\ell} \nabla f \cdot \mathrm{d}\mathbf{r} = \frac{1}{\text{length }(\ell)} f \Big|_{\partial \ell} = \frac{1}{\text{length }(\ell)} [f(b) - f(a)], \tag{2.7}$$

is the discrete gradient. For arbitrary data, there exist a smooth function interpolating it (i.e. taking on its apppropriate point values, averaged tangential components, etc.). Hence, the discrete forms of the vector calculus identities $\nabla \cdot \nabla \times v = 0$ and $\nabla \times \nabla \varphi = 0$ follow using appropriately weighted sums, when the grid used is a simplicial complex [10].

The FVM can also be applied in time to give

$$\int_{t_n}^{t_{n+1}} \int_{\Omega} (\partial_t u + \nabla \cdot f) = 0, \tag{2.8}$$

or

$$\overline{\overline{u}}^{n+1} = \overline{\overline{u}}^{n} + \int_{t_n}^{t_{n+1}} \overline{\overline{\nabla \cdot f}} = \overline{\overline{u}}^{n} + \frac{1}{\text{Vol}(\Omega)} \sum_j \int_{t_n}^{t_{n+1}} A_j \overline{\overline{f_j}}. \tag{2.9}$$

The fluxes $\overline{\overline{f_j}}$ can be approximated directly by incorporating past time levels in standard linear multistep methods or, for hyperbolic equations, by locally solving Riemann problems to estimate the flux across the cell edges [7]. Both these methods conserve the integral of u between time steps even when A_j is nonuniform and time dependent because the structure of (2.9) and consistancy of the difference approximations insure that the solution method is the analog of an integral over the space–time boundary that lies between the spatial grid points and the time levels t_n and t_{n+1}.

In the next two sections we give some specific examples of FVM approximations in one and two space dimensions.

3. One space dimension

Given a mesh $\cdots x_{i-1} < x_i < x_{i+1} < \cdots$, in one space dimension we define

$$\overline{u}_{i+1/2} := \frac{1}{\Delta x_{i+1/2}} \int_{x_i}^{x_{i+1}} u(s)\,\mathrm{d}s, \quad \overline{f}_{i+1/2} := \frac{1}{\Delta x_{i+1/2}} \int_{x_i}^{x_{i+1}} f(u(s), s)\,\mathrm{d}s, \tag{3.1a,b}$$

where the notation $\overline{f}$ means the averaged quantity $\overline{f(u(x), x)}$, Δ is the difference operator $\Delta x_{i+1/2} = x_{i+1} - x_i$. Define $x_{i+1/2} := (x_{i+1} + x_i)/2$. The averaged quantity $\overline{u}_{i+1/2}$ is a second order approximation to the pointwise value $u_{i+1/2} := u(x_{i+1/2})$. To take the derivative of such averaged quantities, we must first extend them from a discrete function to a differentiable one. That is, the average values in (3.1b) must be interpolated to define a smooth function $\overline{f}(x)$, where $\overline{f}(x_{i+1/2}) = \overline{f}_{i+1/2}$. This can be done by defining smooth monotone functions $a(x)$ and $b(x)$ (e.g., piecewise cubic Hermite polynomials with breaks at the mid-mesh points) such that for all i

$$\overline{f}(x) = \frac{1}{b(x) - a(x)} \int_{a(x)}^{b(x)} f(u(s), s)\, ds, \tag{3.2}$$

where

$$a(x_{i+1/2}) = x_i, \quad b(x_{i+1/2}) = x_{i+1}, \quad a'(x_{i+1/2}) = b'(x_{i+1/2}) = 1. \tag{3.3}$$

For example, on an equally spaced grid we could use $a(x) = x - \frac{1}{2}\Delta x$, $b(x) = x + \frac{1}{2}\Delta x$. On unequally spaced grids the monotonicity preserving cubic Hermite interpolants [6] are an excellent choice. Note that the monotonicity of $\{x_i\}$, a and b guarantees that $b - a$ is positive.

If f is continuous, then $\overline{f}$ is differentiable and

$$\partial_x \overline{f}(x) = \frac{f(u(b(x)), b(x))\, b'(x) - f(u(a(x)), a(x))\, a'(x)}{b(x) - a(x)} - \frac{b'(x) - a'(x)}{[b(x) - a(x)]^2} \times \int_{a(x)}^{b(x)} f(u(s), s)\, ds. \tag{3.4}$$

Thus, at the mid-mesh points,

$$\partial_x \overline{f}_{i+1/2} = \frac{\Delta f_{i+1/2}}{\Delta x_{i+1/2}}, \tag{3.5}$$

where $f_i = f(u_i, x_i)$ and $u_i = u(x_i)$ are the values of the functions evaluated at the mesh points.

At the cell edges, the point values of f in eq. (3.5) would be obtained by evaluating f at the point values of u at the cell edges. In the FVM, these values are obtained by differentiating the cumulative integral of u,

$$U(x) = \int_{x_0}^{x} u(s)\, ds. \tag{3.6}$$

That is,

$$u(x) = \partial_x U(x). \tag{3.7}$$

At the grid points U_i is known exactly in terms of the $\overline{u}_{i+1/2}$;

$$U_i = \int_{x_0}^{x_i} u(s)\, ds = \sum_{j=0}^{i-1} \Delta x_{j+1/2}\, \overline{u}_{j+1/2}, \tag{3.8}$$

and

$$\overline{u}_{i+1/2} = \Delta U_{i+1/2} / \Delta x_{i+1/2}. \tag{3.9}$$

This procedure is illustrated graphically in fig. 3.1.

As the $\overline{u}_{i+1/2}$ are the basic FVM quanities, between the grid points, U is approximated by an interpolant. For example, if U is approximated by a piecewise polynomial, then the reconstructed u is also a piecewise polynomial. Typically, U is approximated by a piecewise linear [7], quadratic [14], cubic [14,5], or a œhigher order Hermite interpolant [6,8]. The derivative of a kth degree interpolant at x_i is an $\mathcal{O}((\Delta x)^k)$ FDM approximation to $\partial_x U(x_i)$. In our calculations, we used the derivative of a local kth degree polynomial interpolant of U to approximate $\partial_x U(x_i)$. This can be used in eq. (3.5) to define the pointwise values f_i and f_{i+1} to give

$$\partial_x \overline{f}_{i+1/2} = \frac{f(\partial_x U(x_{i+1}), x_{i+1}) - f(\partial_x U(x_i), x_i)}{\Delta x_{i+1/2}} + \mathcal{O}((\Delta x)^k) \tag{3.10}$$

on smooth meshes and $\mathcal{O}((\Delta x)^{k-1})$ when the mesh is not smooth. This loss of accuracy is illustrated by the examples in section 5.

In many applications u represents density, energy, pressure, concentration or some positive quantity. When u is positive then U must be monotonically increasing, and therefore applying a monotonicity constraint [6] on the numerical derivative approximations of $\partial_x U$ is appropriate. For example, if a cubic Hermite interpolant $\widetilde{U}$ is used to approximate the derivatives, then constraining $\partial_x \widetilde{U}$ to have the same sign as the slope of the data, $S_{i+1/2} = \Delta U_{i+1/2}/\Delta x_{i+1/2}$ $(= \overline{u}_{i+1/2})$, and to satisfy

$$0 \le u_i = |\partial_x \widetilde{U}_i| \le 3 \min(|S_{i+1/2}|, |S_{i-1/2}|) \tag{3.11}$$

guarantees that the resulting interpolant preserves the monotonicity properties of the data points [6].

In some applications u is known to be monotone, consequently U is convex and a convexity constraint [6] such as

$$\min(S_{i+1/2}, S_{i-1/2}) \le \partial_x \widetilde{U}_i \le \max(S_{i+1/2}, S_{i-1/2}) \tag{3.12}$$

is more appropriate.

Next, given u_i, the function values $f(u_i, x_i)$ are evaluated, and the $\partial_x \overline{f}$ are defined by (3.5). Note that applying nonlinear constraints on the derivatives of U, such as (3.11) or (3.12), does not affect the final conservative divergence form of the derivative approximations (3.5) of $\overline{f}$. This would not be the case if first $\partial_x f$ were approximated and then the constraints (3.11) or (3.12) are applied directly to $\partial_x \overline{f}$ (so that the flux f_i out of the ith cell is different than the corresponding f_i into the $(i+1)$st cell) as is sometimes done in FDMs.

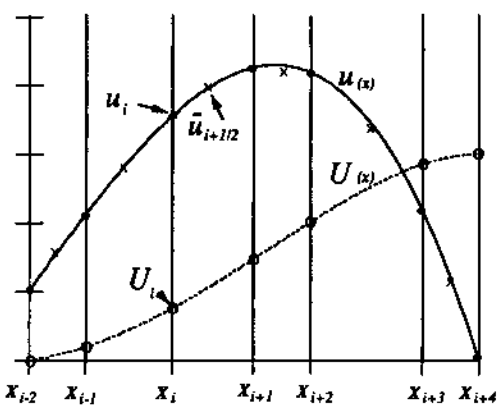

Fig. 3.1. The function u (solid curve) and its cumulative integral U (dashed curve). The values of the cell averages of u are marked with ×'s and the point values by a •. The exact value of U is known at each point marked with a o.

The FVM can also be applied to PDEs with lower order nonlinear terms such as occur in chemically reacting flows:

$$\partial_t \bar{u} + \partial_x \overline{f(u)} = \overline{g(u)}. \tag{3.13}$$

Here $\overline{g(u)}$ may not be well approximated by $g(\bar{u})$ at the mid-mesh points, and this term must also be carefully treated as described in fig. 3.2. It is especially important to treat this term properly when approximating the divergence to fourth (or higher) order, or the overall accuracy of the FVM will be reduced. That is, the high order FVMs require all the terms to be treated consistently. The resulting high order method will require far fewer mesh points in sharp fronts, such as combustion fronts, than a method where the nonlinear terms are not approximated properly. In numerical experiments, we found that the FVM was significantly less accurate when the $g(\bar{u})$ approximation was used.

For higher derivatives of u, the appropriate derivatives of the interpolant of U are used. For example, for second derivatives,

$$\overline{\partial_x^2 u}_{i+1/2} = \frac{\partial_x u_{i+1} - \partial_x u_i}{\Delta x_{i+1/2}} = \frac{\partial_x^2 U_{i+1} - \partial_x^2 U_i}{\Delta x_{i+1/2}}. \tag{3.14}$$

A simple approximation to the first derivative for use in eq. (3.14) is

$$\partial_x u_i = 2(\bar{u}_{i+1/2} - \bar{u}_{i-1/2})/(\Delta x_{i+1/2} + \Delta x_{i-1/2}) + \mathcal{O}(\Delta x). \tag{3.15}$$

On uniform grids the FVM operators simplify to the formulas in table 1. A drawback in mapping directly from $\{\bar{u}_{i+1/2}\}$ to $\{u_i\}$ via these formulas is the lack of a shape preserving constraint step. However, when the solution is well resolved then the shape preserving constraints are usually unnecessary and these formulas are more convenient to use than the two step process. When f is linear, the resulting formulas are equivalent to the standard finite difference formulas in table 2. These are also the same formulas used to derive table 1 by differentiating the cumulative integral of u.

For nonuniform grids, similar direct formulas can be derived for the FVM. For example, a second-order approximation to u_i based on the derivative of a three point quadratic interpolant of U_i is given by the symmetric formula

$$u_i = (\Delta x_{i-1/2}\, \bar{u}_{i+1/2} + \Delta x_{i+1/2} \bar{u}_{i-1/2})/(\Delta x_{i+1/2} + \Delta x_{i-1/2}) + \mathcal{O}((\Delta x)^2) \tag{3.16a}$$

or (similarly) by the one-sided formula

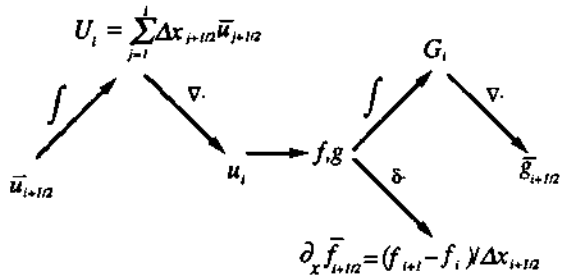

Fig. 3.2. Steps to derive a FVM for eq. (3.13): (1) The cumulative integral U_i is defined at the boundaries of the FV cells. (2) An interpolant of U is constructed and differentiated to define u_i. (3) The functions f_i, g_i are evaluated. (4) The divergence term is evaluated $\partial_x \bar{f}_{i+1/2} = \Delta f_{i+1/2}/\Delta x_{i+1/2}$. (5) The lower order term g is interpolated and integrated to form $G(x) = \int^x g$. (6) The average values $\bar{g}_{i+1/2} = \Delta G_{i+1/2}/\Delta x_{i+1/2}$ are defined.

Table 1
Finite volume method formulas for equally spaced grids, $ch^k(\partial_x)^k u_j = \sum a_{i+1/2}\overline{u}_{(xi+1/2)}$.

Point value	$a_{i-5/2}$	$a_{i-3/2}$	$a_{i-1/2}$	$a_{i+1/2}$	$a_{i+3/2}$	$a_{i+5/2}$	$a_{i+7/2}$	$a_{i+9/2}$	$a_{i+11/2}$	$a_{i+13/2}$	Accuracy
$2u(x_i)$			1	1							$\mathcal{O}(h^2)$
$2u(x_i)$				4	−3	1					$\mathcal{O}(h^2)$
$12u(x_i)$		−1	7	7	−1						$\mathcal{O}(h^4)$
$12u(x_i)$			2	17	−11	5	−1				$\mathcal{O}(h^4)$
$12u(x_i)$				27	−31	25	−11	2			$\mathcal{O}(h^4)$
$60u(x_i)$	1	−8	37	37	−8	1					$\mathcal{O}(h^6)$
$60u(x_i)$		−1	16	72	−43	22	−7	1			$\mathcal{O}(h^6)$
$60u(x_i)$			9	93	−78	57	−28	8	−1		$\mathcal{O}(h^6)$
$60u(x_i)$				156	−267	372	−343	197	−64	9	$\mathcal{O}(h^6)$
$hu_x(x_i)$				−1	1						$\mathcal{O}(h^2)$
$hu_x(x_i)$					−3	6	−4	1			$\mathcal{O}(h^2)$
$12hu_x(x_i)$		1	−15	15	−1						$\mathcal{O}(h^4)$
$12hu_x(x_i)$			−9	0	19	−15	6	−1			$\mathcal{O}(h^4)$
$12hu_x(x_i)$				−44	104	−95	41	−5	−1		$\mathcal{O}(h^4)$
$180hu_x(x_i)$	−2	25	−245	245	−25	2					$\mathcal{O}(h^6)$
$180hu_x(x_i)$		11	−203	175	45	−40	14	−2			$\mathcal{O}(h^5)$
$180hu_x(x_i)$			−126	−56	430	−425	245	−79	11		$\mathcal{O}(h^5)$
$180hu_x(x_i)$				−938	3076	−4835	4655	−2725	893	−126	$\mathcal{O}(h^5)$
$2h^2u_{xx}(x_i)$		1	−1	−1	1						$\mathcal{O}(h^2)$
$2h^2u_{xx}(x_i)$			4	−11	11	−5	1				$\mathcal{O}(h^2)$
$2h^2u_{xx}(x_i)$				9	−29	35	−19	4			$\mathcal{O}(h^2)$
$24h^2u_{xx}(x_i)$	−3	21	−18	−18	21	−3					$\mathcal{O}(h^4)$
$24h^2u_{xx}(x_i)$			45	−123	126	−66	21	−3			$\mathcal{O}(h^4)$
$24h^2u_{xx}(x_i)$				192	−819	1509	−1554	942	−315	45	$\mathcal{O}(h^4)$
$5h^3u_{xxx}(x_i)$		−5	15	−15	5						$\mathcal{O}(h^2)$
$5h^3u_{xxx}(x_i)$			−15	60	−95	75	−30	5			$\mathcal{O}(h^2)$
$5h^3u_{xxx}(x_i)$				−30	130	−225	195	−85	15		$\mathcal{O}(h^2)$

$$u_i = [(2\Delta x_{i+1/2} + \Delta x_{i+3/2})\overline{u}_{i+1/2} - \Delta x_{i+1/2}\,\overline{u}_{i+3/2}]/(\Delta x_{i+1/2} + \Delta x_{i+3/2}) + \mathcal{O}((\Delta x)^2). \tag{3.16b}$$

Higher order formulas can be generated by using higher degree interpolants. In the examples in section 7 we also used five point local polynomial quartic interpolants.

Table 2
Finite difference method formulas for equally spaced grids: $ch^k(\partial_x)^k u_j = \sum a_i U(x_i)$.

Derivative	a_{i-3}	a_{i-2}	a_{i-1}	a_i	a_{i+1}	a_{i+2}	a_{i+3}	a_{i+4}	a_{i+5}	a_{i+6}	Accuracy
$2hU_x(x_i)$			−1		1						$\mathcal{O}(h^2)$
$2hU_x(x_i)$				−3	4	−1					$\mathcal{O}(h^2)$
$12hU_x(x_i)$		1	−8		8	−1					$\mathcal{O}(h^4)$
$12hU_x(x_i)$			−3	−10	18	−6	1				$\mathcal{O}(h^4)$
$12hU_x(x_i)$				−25	48	−36	16	−3			$\mathcal{O}(h^4)$
$60hU_x(x_i)$	−1	9	−45		45	−9	1				$\mathcal{O}(h^6)$
$60hU_x(x_i)$		2	−24	−35	80	−30	8	−1			$\mathcal{O}(h^6)$
$60hU_x(x_i)$			−10	−77	150	−100	50	−15	2		$\mathcal{O}(h^6)$
$60hU_x(x_i)$				−147	360	−450	400	−225	72	−10	$\mathcal{O}(h^6)$
$h2U_{xx}(x_i)$			1	−2	1						$\mathcal{O}(h^2)$
$h2U_{xx}(x_i)$				2	−5	4	−1				$\mathcal{O}(h^2)$
$12h2U_{xx}(x_i)$		−1	16	−30	16	−1					$\mathcal{O}(h^4)$
$12h2U_{xx}(x_i)$			10	−15	−4	14	−6	1			$\mathcal{O}(h^4)$
$12h2U_{xx}(x_i)$				35	−104	114	−56	11			$\mathcal{O}(h^3)$
$180h^2U_{xx}(x_i)$	2	−27	270	−490	270	−27	2				$\mathcal{O}(h^6)$
$180h^2U_{xx}(x_i)$		−13	228	−420	200	15	−12	2			$\mathcal{O}(h^5)$
$180h^2U_{xx}(x_i)$			137	−147	−255	470	−285	93	−13		$\mathcal{O}(h5)$
$180h^2U_{xx}(x_i)$				812	−3132	5265	−5080	2970	−972	137	$\mathcal{O}(h^5)$
$2h^3U_{xxx}(x_i)$		−1	2		−2	1					$\mathcal{O}(h^2)$
$2h^3U_{xxx}(x_i)$			−3	10	−12	6	−1				$\mathcal{O}(h^2)$
$2h^3U_{xxx}(x_i)$				−5	18	−24	14	−3			$\mathcal{O}(h^2)$
$h^4U_{xxxx}(x_i)$		1	−4	6	−4	1					$\mathcal{O}(h^2)$
$h^4U_{xxxx}(x_i)$			2	−9	16	−14	6	−1			$\mathcal{O}(h^2)$
$h^4U_{xxxx}(x_i)$				3	−14	26	−24	11	−2		$\mathcal{O}(h^2)$

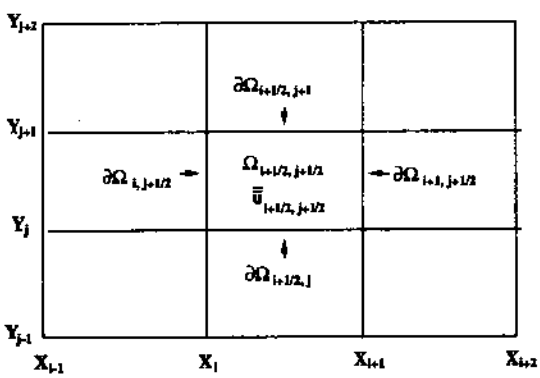

Fig. 4.1. The boundaries of $\Omega_{i+1/2,j+1/2}$ are given by the grid lines. $U(x,y)$ is known exactly where the grid lines intersect. The boundaries of the cell, $\partial\Omega_{i+1,j+1/2}$, $\partial\Omega_{i+1/2,j}$, $\partial\Omega_{i+1/2,j+1}$, and $\partial\Omega_{i,j+1/2}$ lie on the grid lines.

4. Two space dimensions

4.1. Orthogonal grids

The one-dimensional formulas generalize easily to FVMs on tensor product (x_i, y_j) grids, such as the one shown in fig. 4.1. The average values within the mesh cells are

$$\bar{\bar{u}}(x_{i+1/2},y_{j+1/2}) := \frac{1}{\Delta x_{i+1/2}\Delta y_{j+1/2}} \int_{x_i}^{x_{i+1}} \mathrm{d}r \int_{y_j}^{y_{j+1}} \mathrm{d}s\, u(r,s) = \frac{1}{A_{i+1/2,j+1/2}} \int_{\Omega_{i+1/2,j+1/2}} u. \tag{4.1}$$

Here $\Omega_{i+1/2,j+1/2}$ is the rectangle with corners (x_i,y_j), (x_i,y_{j+1}), (x_{i+1},y_j) and (x_{i+1},y_{j+1}) with area $A_{i+1/2,j+1/2} = \Delta x_{i+1/2}\Delta y_{j+1/2}$. The function is extended to the region between the grid points by defining monotone functions a, b, $c(y)$ and $d(y)$ that satisfy (3.2) and

$$c(y_{j+1/2}) = y_j,\ d(y_{j+1/2}) = y_{j+1},\quad c'(y_{j+1/2}) = d'(y_{j+1/2}) = 1, \tag{4.2}$$

and

$$\bar{\bar{u}}(x,y) = \frac{1}{[b(x)-a(x)][d(y)-c(y)]} \int_{a(x)}^{b(x)} \mathrm{d}r \int_{c(y)}^{d(y)} \mathrm{d}s\, u(r,s). \tag{4.3}$$

Proceeding as in the 1D case, we define

$$U(x,y) = \int_{x_0}^{x} \mathrm{d}r \int_{y_0}^{y} \mathrm{d}s\, u(r,s) \tag{4.4}$$

and

$$U(x_i,y_j) := U_{i,j} = \sum_{k=1}^{i-1}\sum_{\ell=1}^{j-1} \Delta x_{k+1/2}\Delta y_{\ell+1/2}\bar{\bar{u}}_{k+1/2,\ell+1/2}. \tag{4.5}$$

U and its partial derivatives can be obtained by the 1D local polynomial interpolation techniques in table 2, applied separately in the x and y direction.

Divergence

The FVM approximation of the divergence is calculated using (2.4) to give

$$\begin{aligned}\overline{\overline{\nabla\cdot f}}_{i+1/2,j+1/2} &:= \frac{1}{A_{i+1/2,j+1/2}} \int_{\partial\Omega_{i+1/2,j+1/2}} f\cdot\hat{n} \\ &= \frac{\bar{f}_{i+1,j+1/2}\Delta y_{j+1/2} - \bar{f}_{i,j+1/2}\Delta y_{j+1/2} + \bar{f}_{i+1/2,j+1}\Delta x_{i+1/2} - \bar{f}_{i+1/2,j}\Delta x_{i+1/2}}{\Delta x_{i+1/2}\Delta y_{j+1/2}},\end{aligned} \tag{4.6}$$

where $\hat{n}$ is the unit outward normal to the boundary and $\bar{f}_{i,j+1/2}$ can be interperted as the mean value of $f\cdot\hat{n}$ over the boundary $\partial\Omega_{i,j+1/2}$ as shown in fig. 4.1. The other terms are defined in a similar fashion.

The boundary integral can be approximated on each of the four edges by first approximating average values for u at the edges of the cells. For example, a second-order approximation, similar to (3.16a), for the average of u over the edge of $\Omega_{i+1/2,j+1/2}$ between the points (x_i,y_j) and (x_{i+1},y_j) is

$$\overline{u}_{i+1/2,j} = \frac{1}{\Delta x_{i+1/2}} \int_{x_i}^{x_{i+1}} \mathrm{d}r\, u(r, y_j) \approx \frac{\Delta y_{j-1/2}\overline{\overline{u}}_{i+1/2,j+1/2} + \Delta y_{j+1/2}\overline{\overline{u}}_{i+1/2,j-1/2}}{\Delta y_{j-1/2} + \Delta y_{j+1/2}}. \tag{4.7}$$

Using these, the pointwise values of u at the cell corners are, to second order, given by the following extension of (3.16a):

$$\begin{aligned} u_{i,j} &\approx \frac{\Delta x_{i-1/2}\overline{u}_{i+1/2,j} + \Delta x_{i+1/2}\overline{u}_{i-1/2,j}}{\Delta x_{i-1/2} + \Delta x_{i+1/2}} \\ &\approx (\Delta x_{i-1/2}\Delta y_{j-1/2}\overline{\overline{u}}_{i+1/2,j+1/2} + \Delta x_{i-1/2}\Delta y_{j+1/2}\overline{\overline{u}}_{i+1/2,j-1/2} \\ &\quad + \Delta x_{i+1/2}\Delta y_{j-1/2}\overline{\overline{u}}_{i-1/2,j+1/2} + \Delta x_{i+1/2}\Delta y_{j+1/2}\overline{\overline{u}}_{i-1/2,j-1/2}) \\ &\quad \times [(\Delta x_{i-1/2} + \Delta x_{i+1/2})(\Delta y_{j-1/2} + \Delta y_{i+1/2})]^{-1}. \end{aligned} \tag{4.8}$$

Next $f(u)$ is evaluated at the pointwise values and f is integrated along each edge using the one-dimensional quadrature formulas. If the trapezoidal rule is used, then the integration along the right edge is simply

$$\Delta y_{j+1/2}\overline{f}^{x}_{i+1,j+1/2} = \int_{\partial\Omega_{i+1,j+1/2}} f \cdot \hat{n} \approx \tfrac{1}{2}\Delta y_{j+1/2}(f^x_{i+1,j+1} + f^x_{i+1,j}) \tag{4.9}$$

and on the upper edge

$$\Delta x_{i+1/2}\overline{f}^{y}_{i+1/2,j+1} = \int_{\partial\Omega_{i+1/2,j+1}} f \cdot \hat{n} \approx \tfrac{1}{2}\Delta x_{i+1/2}(f^y_{i+1,j+1} + f^y_{i,j+1}), \tag{4.10}$$

where f^x is the component of f in the x-direction and f^y is the component in the y-direction. Alternatively, Simpson's rule for uniform spacing

$$\overline{f}^{x}_{i+1,j+1/2} \approx \tfrac{1}{6}(f^x_{i+1,j+1} + 4f^x_{i,j+1/2} + f^x_{i+1,j}) \tag{4.11}$$

could be used with an appropriate definition of $f^x_{i,j+1/2}$.

The integral along the entire cell boundary gives the second order approximation for the average value of the divergence

$$\begin{aligned} \overline{\overline{\nabla \cdot f}} \approx [&\Delta y_{i+1/2}(\overline{f}^{x}_{i+1,j+1/2} - \overline{f}^{x}_{i,j+1/2}) + \Delta x_{j+1/2}(\overline{f}^{y}_{i+1/2,j+1} - \overline{f}^{y}_{i+1/2,j})]/ \\ &(\Delta x_{i+1/2}\Delta y_{j+1/2}). \end{aligned} \tag{4.12}$$

The simplest second-order approximation for the contour integral is by the trapezoidal rule. However, using Simpson's rule, a nine point scheme can be designed so that for linear functions $f(u,v) = (u,v)$ the truncation error on uniform grids ($h = \Delta x = \Delta y$) for $\overline{\overline{\nabla \cdot (u,v)}}$ is given by $\frac{1}{6}h^2\Delta\nabla \cdot (u,v)$ which is isotropic to fourth order. A second-order FVM with fourth-order isotropic errors preserves the symmetry of the differential operator better than other second-order approximations. Although the convergence rate is still second-order, nonsymmetries caused by grid orientation effects are isotropic to fourth order. That is, orientation effects of, say, shock waves travelling at different angles with

respect to the mesh are smaller than for other second-order approximations. Even so, our numerical examples show that the symmetric second-order methods are still much less accurate than a good fourth-order approximation. An advantage of (4.12) is that the simple form of the error makes deferred correction approximations easy. (In a deferred correction method, first $\nabla \cdot f$ is approximated, then $\frac{1}{6}h^2\Delta_h(\nabla_h \cdot f)$ is evaluated and subtracted off to give a fourth-order approximation.)

The second-order method with error isotropic to fourth order is found by finding an appropriate interpolant to $u_{i,j+1/2}$ and the usual flux formulas to find $u_{i,j}$ and $u_{i,j+1}$, and then using Simpson's rule (4.11) for the integral along the cell boundary. The pointwise values will be approximated by

$$u_{i,j+1/2} = a_{-1}(\bar{\bar{u}}_{i+1/2,j+3/2} + \bar{\bar{u}}_{i-1/2,j+3/2}) + a_0(\bar{\bar{u}}_{i+1/2,j+1/2} + \bar{\bar{u}}_{i-1/2,j+1/2}) + a_1(\bar{\bar{u}}_{i+1/2,j-1/2} + \bar{\bar{u}}_{i+1/2,j-1/2}). \tag{4.13}$$

For second order accuracy $a_{-1} = a_1$ and $a_{-1} + a_0 + a_1 = 1$. This leaves one parameter free to adjust the second order truncation error. If we choose $a_0 = 3/4$, $a_{-1} = 1/8$, $a_1 = 1/8$ the second order truncation error is given by $\frac{1}{6}h^2\Delta\nabla \cdot (u, v)$ as desired. For $\nabla f(u, v)$ the normal component of the function evaluated at the pointwise values can replace the values of u and v above, though the formula is only isotropic if the function is linear.

On a nonuniform grid it is not generally possible to derive a FVM with a leading order error term which is isotropic. However, it is possible to choose an approximation to $u_{i,j+1/2}$ which approaches the one described above for uniform grids as the grid approaches uniformity. For the pointwise value $u_{i,j+1/2}$ to be second order accurate $a_{-1} + a_0 + a_1 = 1$ and $a_1(\Delta y_{j+3/2} + \Delta y_{j+1/2}) - a_{-1}(\Delta y_{j+1/2} + \Delta y_{j-1/2}) = 0$. There is a one parameter family of solutions to these which gives (4.12) on a uniform grid. One simple effective choice is simply to weigh the middle coefficient by the relative cell length;

$$a_0 = \frac{9}{4}\frac{\Delta y_{j+1/2}}{\Delta y_{j+3/2} + \Delta y_{j+1/2} + \Delta y_{j-1/2}}, \quad a_{-1} = (1 - a_0)\frac{\Delta y_{j+1/2} + \Delta y_{j+3/2}}{\Delta y_{j+3/2} + 2\Delta y_{j+1/2} + \Delta y_{j-1/2}},$$

$$a_1 = (1 - a_0)\frac{\Delta y_{j+1/2} + \Delta y_{j-1/2}}{\Delta y_{j+3/2} + 2\Delta y_{j+1/2} + \Delta y_{j-1/2}};$$

$u_{i+1,j+1/2}$ is found using the same coefficients. For $v_{i+1/2,j}$ and $v_{i+1/2,j+1}$ use coefficients b_k, $k = -1, 0, 1$ where b_k is given by the formula for a_k with Δy's replaced by the correspon ing Δx's.

Gradient and curl

The FVM gradient is obtained by integrating along the grid edges. Let $\Delta x_{i+\frac{1}{2},j} = x_{i+1,j} - x_{i,j}$ denote the difference in the x coordinate of the gridpoints (i, j) and $(i + 1, j)$, with a similar notation for the vertical edges. The FVM gradient is

$$\bar{\nabla} f_{i+1/2,j} := \frac{\Delta f_{i+1/2,j}}{\Delta x_{i+1/2,j}}, \tag{4.14a}$$

$$\bar{\nabla} f_{i,j+\frac{1}{2}} := \frac{\Delta f_{i,j+\frac{1}{2}}}{\Delta y_{i,j+\frac{1}{2}}}, \tag{4.14b}$$

while the FVM curl is

$$\overline{\overline{\nabla \times v}}_{i+1/2,j+1/2} := \frac{\overline{v_x}_{i+1/2,j} \cdot \Delta x_{i+1/2,j} + \overline{v_y}_{i+1,j+1/2} \cdot \Delta y_{i+1,j+1/2} - \overline{v_x}_{i+1/2,j+1} \cdot \Delta x_{i+1/2,j+1} - \overline{v_y}_{i,j+1/2} \cdot \Delta y_{i,j+1/2}}{A_{i+1/2,j+1/2}}, \tag{4.14c}$$

where $\overline{v}_x$ is mean-value of the x-component of the vector $\overline{v}$.

When f is a composed function, the same manipulations as in the previous section may be performed to determine the quadrature rules.

We point out that these discrete operators do not correspond directly to the usual differential operators. For example, the gradient maps scalar functions on the gridpoints to scalar functions on the edges, *not* vector functions. Thus, there are two types of scalar data: those that live on vertical and horizontal edges. On nondegenerate grids the gradient components can be interpolated and combined to get a vector gradient. However, often it is not the full gradient vector which is needed, only the normal or tangential component as in the following section on the Laplacian operator.

This FVM technique works in any number of dimensions, and satisfies discrete analogues of the vector identities *exactly*. This follows from general principles in algebraic topology: namely that the boundary of a boundary is null, as explained in detail in [10]. Also there we show that if the Laplacian is computed as a FVM differential operator composed with its adjoint then Hodge's theorem applies: namely we can compute the dimension of the kernel of the Laplacian in terms of the topology of the underlying manifold. This corresponds to the reasoning of using a FVM gradient, and then using its adjoint as a divergence instead of a FVM divergence.

In addition, this method can be used to compute the vector Laplacian. Unfortunately, using this approach, the resulting Laplacian is not local, since the adjoint process does not preserve the localness of operators.

Laplacian

The FVM approximation of

$$\overline{\overline{\nabla \cdot \mathrm{d}\nabla u}}_{i+1/2,j+1/2} := \frac{1}{A_{i+1/2,j+1/2}} \int_{\partial\Omega_{i+1/2,j+1/2}} \mathrm{d}\nabla u \cdot \hat{n} \tag{4.15}$$

can be constructed by approximating directional derivative (mean flux) at the midpoints of the cell edges using

$$\overline{\mathrm{d}\nabla u_{i,j+1/2} \cdot \hat{n}_x} = \overline{d}_{i,j+1/2} \frac{\overline{\overline{u}}_{i+1/2,j+1/2} - \overline{\overline{u}}_{i-1/2,j+1/2}}{x_{i+1/2} - x_{i-1/2}} + O(\Delta x) \tag{4.16}$$

and similar formulas. Here $\hat{n}_x$ denotes the unit vector in the x direction and

$$\overline{d}_{i,j+1/2} = 2\overline{\overline{d}}_{i+1/2,j+1/2}\overline{\overline{d}}_{i-1/2,j+1/2}(\overline{\overline{d}}_{i+1/2,j+1/2} + \overline{\overline{d}}_{i-1/2,j+1/2})^{-1}. \tag{4.17}$$

The harmonic average is used to insure the continuity of the flux across the cell edge when the diffusion coefficient is discontinuous [12]. We assume the harmonic averages of the scalar diffusion coefficient

$$\overline{\overline{d}}_{i+1/2,j+1/2} := \frac{1}{A_{i+1/2,j+1/2}} \left(\int_{\Omega_{i+1/2,j+1/2}} d^{-1} \right)^{-1} \tag{4.18}$$

are known. Often the integrals in (4.18) to define $\overline{\overline{d}}$ are calculated numerically on a much finer mesh than the mesh used to solve the FVM approximation. This calculation is done once to define $\overline{\overline{d}}$ on the coarser mesh at the beginning of the problem and then the finer mesh is eliminated.

Equation (4.16) defines a midpoint rule approximation of the mean flux through the cell boundary. The approximations in nearby cells can be combined to give more accurate and symmetric formulas. The directional derivatives at the cell corners are useful quantities in deriving these approximations and can be approximated using (4.16):

$$\begin{aligned} d\nabla u_{i,j} \cdot \hat{n}_x &= \frac{\Delta y_{j-1/2} \overline{d\nabla u_{i,j+1/2} \cdot \hat{n}_x} + \Delta y_{j+1/2} \overline{d\nabla u_{i,j-1/2} \cdot \hat{n}_x}}{\Delta y_{j+1/2} + \Delta y_{j-1/2}}, \\ d\nabla u_{i,j} \cdot \hat{n}_y &= \frac{\Delta x_{i-1/2} \overline{d\nabla u_{i+1/2,j} \cdot \hat{n}_y} + \Delta x_{i+1/2} \overline{d\nabla u_{i-1/2,j} \cdot \hat{n}_y}}{\Delta x_{i+1/2} + \Delta x_{i-1/2}} \end{aligned} \tag{4.19}$$

To evaluate the mean flux $f(u) = \overline{d(x)u_x}$ in terms of the volume averages $\overline{\overline{u}}$, first the volume averages are used to approximate the pointwise values of u and then $f(u)$ can be approximated in two distinct ways: We could first interpolate u to form $\tilde{u}$ along the volume boundary. Next analytically (or numerically) evaluate $\int_{\partial\Omega} f(\tilde{u}) \cdot \boldsymbol{n}$. Alternately, we could have first evaluated $f(u)$ at the grid points, then interpolated and integrated $\tilde{f}$ along the volume boundary. In our numerical experiments, the more accurate method depended on whether u or f is smoother.

When d is constant it is possible, as it was for the divergence, to find a second-order approximation to Δu which has isotropic truncation error $\frac{1}{12}h^2\Delta^2 u$ on uniform grids ($h = \Delta x = \Delta y$). We find an interpolant for the cell midpoint such that the integration can be done using Simpson's rule (4.11):

$$\begin{aligned} \partial_x u_{i,j+1/2} = {} & a_{-1}(\overline{\overline{u}}_{i+1/2,j+3/2} - \overline{\overline{u}}_{i-1/2,j+3/2}) + a_0(\overline{\overline{u}}_{i+1/2,j+1/2} - \overline{\overline{u}}_{i-1/2,j+1/2}) \\ & + a_1(\overline{\overline{u}}_{i+1/2,j-1/2} - \overline{\overline{u}}_{i-1/2,j-1/2}). \end{aligned} \tag{4.20}$$

For second-order accuracy $a_{-1} = a_1$ and $a_{-1} + a_0 + a_1 = 1$. This leaves one parameter free to adjust the second-order truncation error. For the Laplacian, the error is isotropic if we choose $a_0 = 1, a_{-1} = 0, a_1 = 0$. The nine-point stencil of the resulting scheme is given by

$$\begin{array}{ccc} \frac{1}{6h^2} & \frac{4}{6h^2} & \frac{1}{6h^2} \\ \frac{4}{6h^2} & -\frac{20}{6h^2} & \frac{4}{6h^2} \\ \frac{1}{6h^2} & \frac{4}{6h^2} & \frac{1}{6h^2} \end{array} \tag{4.21}$$

As for the second-order isotropic divergence operator, one defect correction iteration can raise the method to fourth order. We extend the method to nonuniform grids in the same fashion as for the divergence. For the Laplacian, the restriction on the coefficients is the same and the simple weighting method has the coefficients

$$a_0 = \frac{3\Delta y_{j+1/2}}{\Delta y_{j+3/2} + \Delta y_{j+1/2} + \Delta y_{j-1/2}}, \quad a_{-1} = (1 - a_0)\frac{\Delta y_{j+1/2} + \Delta y_{j+3/2}}{\Delta y_{j+3/2} + 2\Delta y_{j+1/2} + \Delta y_{j-1/2}},$$

$$a_1 = (1 - a_0)\frac{\Delta y_{j+1/2} + \Delta y_{j-1/2}}{\Delta y_{j+3/2} + 2\Delta y_{j+1/2} + \Delta y_{j-1/2}}$$

$u_{i+1,j+1/2}$ is found using the same coefficients. For $v_{i+1/2,j}$ and $v_{i+1/2,j+1}$ use coefficients b_k, $k = -1, 0, 1$ where b_k is given by the formula for a_k with Δy's replaced by the corresponding Δx's. As mentioned for the divergence this a simple but not necessarily optimal choice for the coefficients.

4.2. Nonorthogonal grids

The accuracy of the FVM depends upon being able to accurately calculate the contour integral. This requires picking the control volume so the boundary integral can be accurately approximated with the available data on nonorthogonal grids. If the boundary of the control volume is divided into four segments, as shown in fig. 4.1, the data at the six points surrounding each segment can be used in approximating its contribution to the boundary integral and the resulting difference formula will have a nine point stencil. Six data points also uniquely define a quadratic if they do not all lie on a conic section. If they lie near a conic section, then the quadratic is nearly degenerate and the difference approximation is ill conditioned (see appendix B). On tensor product grids the mesh points are aligned on two straight lines, a degenerate conic. However, there is a fortunate cancellation of the truncation errors in the boundary integral approximations on opposite sides of the control volume and the final FVM approximation is exact for quadratics.

In the FVM approximation of the Laplacian $\nabla u \cdot \hat{n}$ must be computed along the control volume boundary. If the six points do not lie on a conic section, ∇u is known everywhere and FVM approximation is easily computed. If the points are on a conic section, then ∇u is known only at the center of the conic. For tensor product grids, this requires the control volume to pass through cell centers.

On more general grids, because only $\nabla u \cdot \hat{n}$ is needed on the cell boundary, it is conceiveable that an approximation for $\nabla u \cdot \hat{n}$ exists, which is exact for quadratics although none does for ∇u (see appendix B).

The development of FVM's on arbitrary grids which respect the vector identities will require the tools of algebraic topology [10]. The idea is the following: The operators of Div, Grad, and Curl, correspond to the exterior derivative d acting on differential forms. The vector identities correspond to the fact that $d \circ d = 0$. To mimic this, we require the grid to be a triangulation of the underlying manifold by a chain complex, transform vector and scalar quatities into forms and use integration of the forms over cells of appropriate dimension to encode them as discrete k-cell quantities. For example, in two dimensions, scalar functions are encoded as the evaluation of scalar functions on the grid points (the 0-cells). Vector functions are encoded as the integral of a 1-form along a grid edge (a 1-cell). Area cell quantities are encoded as the integral of a 2-form over a grid cell (a 2-cell). This process is known as the DeRham map from the DeRham complex to the cochain complex. The discrete versions of Div, Grad, and Curl, correspond closely with the coboundary operator and are determined by Stokes' theorem; let ω be a differential k-form, and Ω a $k + 1$-cell, and denote by brackets the pairing between differential forms and cells determined by integrating the form over a cell. In this notation, the general form of Stokes' theorem is

$$\langle d\omega, \Omega \rangle = \langle \omega, \partial\Omega \rangle \tag{4.22}$$

where ∂ is the boundary operator. By assuming constancy on $k+1$-cells, the FVM exterior derivative is

$$d\omega|_{\Omega} = \frac{\langle d\omega, \Omega \rangle}{\mathrm{Vol}(\Omega)} = \frac{\langle \omega, \partial\Omega \rangle}{\mathrm{vol}(\Omega)} = \frac{\int_{\partial\Omega} \omega}{\mathrm{vol}(\Omega)}. \tag{4.23}$$

The vector identities follow from the fact that the coboundary operator δ, being the adjoint of ∂, also satisfies $\delta \circ \delta = 0$.

5. Examples

We test the FVM on two two-dimensional evolution equations: a unidirectional wave equation

$$u_t = \nabla \cdot (u, u) = u_x + u_y \tag{5.1}$$

and the diffusion equation

$$u_t = \Delta u = u_{xx} + u_{yy}. \tag{5.2}$$

Both equations were solved with Gaussian initial data and periodic boundary conditions on a square domain in the (x, y) plane. Tensor product grids were used with uniform, random or exponential spacing in the two directions.

We integrated both equations with a variable time step fourth-order Adams–Bashforth–Moulton method. The errors due to time discretization were negligible compared to errors due to spatial discretization. The cumulative integrals in the FVMs were differentiated using local quadratic, eq. (3.16), or quartic [9] polynomial interpolation. For these linear PDEs, on uniform grids, these methods are equivalent to the standard FDMs in table 2. We will refer to them by their order of accuracy on a uniform grid.

5.1. Wave equation

We first test the order of accuracy of the divergence operator on random tensor product grids on the function $f(x, y) = (e^{x+y}, e^{x+y})$ by comparing the maximum error of the FVM approximation to the known local mean values of the divergence $2e^{x+y}$. The random grids were generated by defining the position of the x coordinate of the j^{th} grid point as $(j + R_j\eta)\,\Delta x$. Here Δx is the average grid spacing, $R_j \in (-1/2, 1/2)$ is a random sequence, and $\eta < 1$ is a parameter determining the relative size of the perturbations from the uniform grid. The position of the y-coordinate is computed in a similar way.

In fig. 5.1 we plot the log of the maximum error in the local mean divergence versus the log of the maximum mesh spacing for second- and fourth-order FVM's represented by open and solid symbols respectively. Each cluster of points represents a different random sequence perturbing uniform grids of various sizes. For each value of η, we show a least squares linear fit of the data. The slope of this linear fit is an approximation to the asymptotic order of accuracy of the method. For uniform grids ($\eta = 0$ represented by the square boxes), we confirm that the methods are second- and fourth-order accurate. As the grid becomes rougher ($\eta = 0.05$, 0.2, and 1.0) the methods degrade by one order because the exact cancellations which occur on uniform grids is lost. The second-order FVM reduces

to first order on the random grid and the fourth-order FVM degenerates to third order. Also, for the very rough (near singular) grids, the scatter in the data becomes greater and the constant in the error term increases. That is, although the approximations on the $\eta = 0.2$ and $\eta = 1.0$ grids converge at the same rate, the maximum errors on the rougher grid ($\eta = 1.0$) are up to five times larger.

In all our numerical experiments, the magnitude of the error for the fourth-order FVM is much smaller than the error for the second-order FVM on the same grid. In this example, the errors of the fourth-order method were 0.01% of the errors of the second-order method. This has long been known for FDM's on uniform grids and illustrates the superiority of fourth-order methods to second-order methods over wide ranges of resolution and grid smoothness.

Next, we solved eqn. (5.1) with periodic boundary conditions on a very rough random grid ($\eta = 0.9$). Neglecting the boundary conditions, the Gaussian shape of the analytic solution, $u(x,y,t) = \exp\{-5[(x+t)^2 + (y+t)^2]\}$, is preserved and translates at speed -1 in the x and y directions. Because of the periodic boundary conditions, the solution at times $t = 0, 2, 4, 6, 8, \ldots$ are identical to the initial condition. The initial condition and the random grid are shown in fig. 5.2.

Fig. 5.3 shows the solution computed using the conservative centered FDM approximation,

$$\nabla \cdot (u,u)_{i,j} \approx \frac{u_{i+1,j} - u_{i-1,j}}{x_{i+1,j} - x_{i-1,j}} + \frac{u_{i,j+1} - u_{i,j-1}}{x_{i,j+1} - x_{i,j-1}}. \tag{5.3}$$

This method does not accurately take the variation in cell volumes into account. The solution is poor at $t = 2$, fig. 5.3a, and even worse at $t = 8$, fig. 5.3b. Much of the error comes from grid effects.

Fig. 5.4 shows the solution computed with the second-order FVM approximation. The integrals along the cell boundaries are constructed using eq. (4.7). At $t = 2$, fig. 5.4a, the solution is much better than when computed using the FDM method. By $t = 8$, fig. 5.4b, while the solution is slightly less distorted than the one computed using the FDM, it is a very poor approximation of the true solution shown in fig. 5.2.

Fig. 5.5 shows the solution at $t = 2$ and $t = 8$ computed using the fourth-order FVM constructed by using the one-dimensional fourth-order flux formulas to get the cell boundary integrals (a fourth-order analogue of eq. (4.7)). At $t = 2$, the solution is quite accurate. Some amplitude has been lost, but the shape and position of the peak are excellent. At $t = 8$, the solution is still much better than the second-order method, but some grid effects have crept in. This is seen in the change in shape and the appearance of dips behind the peak (similar to those seen for the second-order method but much smaller in magnitude).

The conlusion to be drawn from this example is that while the second-order FVM does slightly better than the second-order FDM, the fourth-order FVM is a more accurate and has much smaller variable grid effects.

5.2. *Diffusion equations*

We test the order of accuracy of the Laplacian operator on random tensor product grids for the function $f(x,y) = e^{x+y}$ by comparing the FVM approximation to the known Laplacian $2e^{x+y}$. In fig. 5.6 we plot the log of the maximum error in the localized mean divergence versus the log of the maximum mesh spacing for second and fourth-order FVM's represented by open and solid symbols respectively. Each cluster of points in fig. 5.6 represents a different random sequence perturbing uniform grids of various sizes. For each value of η, we show a least squares linear fit of the data. The slope of this least squares fit is an approximation to the asymptotic order of accuracy of the method.

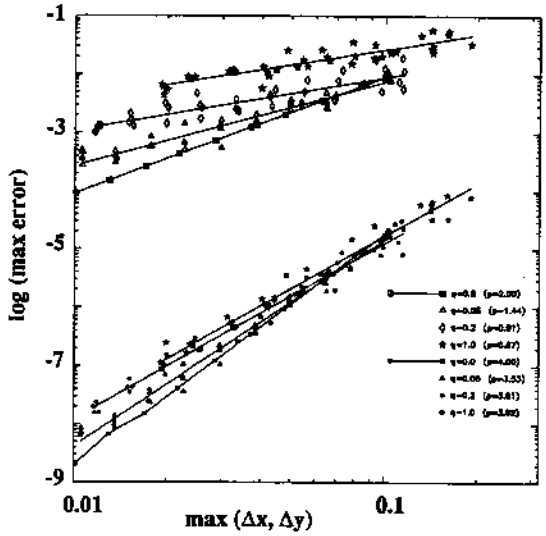

Fig. 5.1. Test of accuracy of the second- and fourth-order FVM divergence on random grids with $\eta = 0.0$, 0.05, 0.2, and 1.0 using the test function (e^{x+y}, e^{x+y}). For these grids, the approximate orders (the slope of the least-squares line fit) for the second-order FVM are 2.00, 1.44, 0.91, and 0.87. The corresponding convergence rates for the fourth-order FVM are 4.00, 3.53, 3.01 and 3.02.

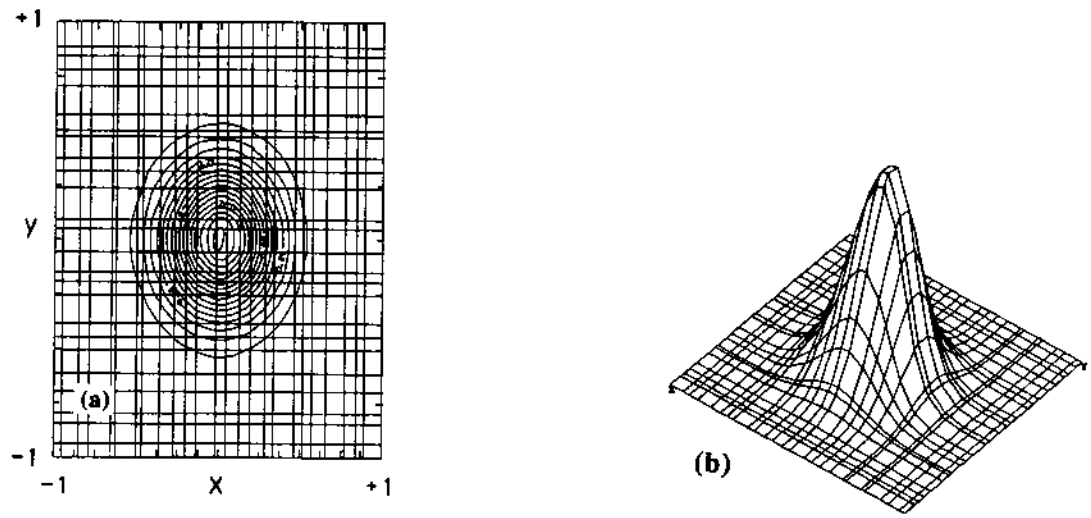

Fig. 5.2. The initial condition $u = \exp[-5(x^2 + y^2)]$ used with eq. (5.1). (a) shows a contour plot of the solution and the random grid with $\eta = 0.9$. (b) shows a surface plot of the initial condition. This is also the solution at $t = 2, 4, 6, \ldots$.

For uniform grids ($\eta = 0$ represented by the square boxes) we confirm that the methods are second and fourth-order accurate. As the grid becomes rougher ($\eta = 0.05$, 0.2, and 1.0) the methods degrade by more than two orders. In fact, the second-order FVM is not consistent as the maximum spacing in a random mesh is reduced to zero and the fourth-order FVM drops to only slightly better than first order.

For the very rough (near singular) grids, the scatter in the data becomes greater and the constant in the error term increases. That is, although the approximations on the $\eta = 0.2$ and $\eta = 1.0$ grids converge at the same rate, the maximum errors on the rougher grid ($\eta = 1.0$) are up to five times larger. In all cases shown, the magnitude of the error is much smaller for the fourth-order FVM.

We computed the solution to the diffusion equation using the same initial condition as for the wave equation. The exponentially graded grid and initial conditions are shown in fig. 5.7. The x-grid spacing of the exponential grid is determined by partitioning the interval [0.7,1] into a sequence of

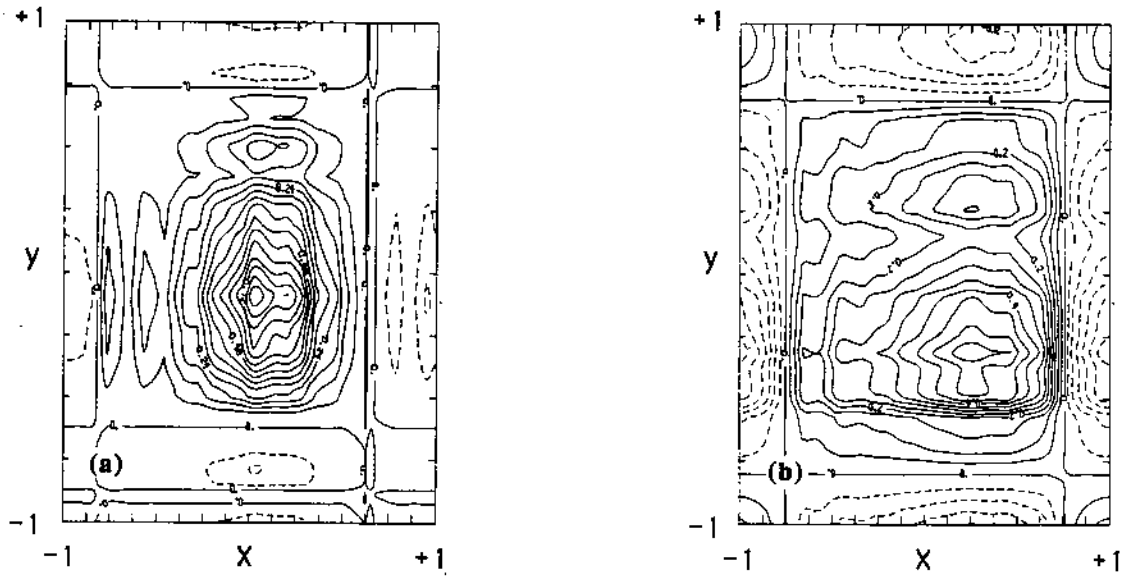

Fig. 5.3. Contour plot of the solution of eq. (5.1) starting with the initial condition and random grid shown in fig. 5.2. The divergence was approximated using the second-order centered FDM method (5.3). The solution is shown at time $t = 2$ in fig. (a) and at time $t = 8$ in (b).

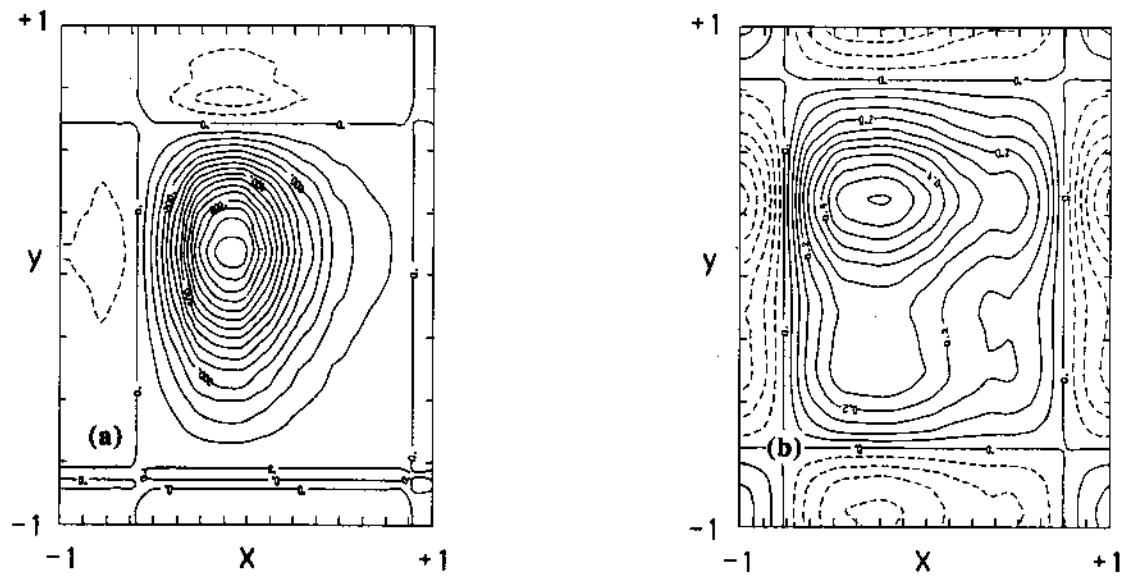

Fig. 5.4. Contour plot of the solution of eq. (5.1) starting with the initial condition and random grid shown in fig. 5.2. The divergence was approximated using the second-order centered FVM method (4.7). The solution is shown at time $t = 2$ in fig. (a) and at time $t = 8$ in (b).

cells $C_1 \cup C_2 \ldots C_k$, so that the left hand endpoint of C_1 is 0.7 and the right hand endpoint of C_k is 1 and $\ell(C_1) = r\ell(C_{i-1})$ where ℓ denotes the length and r is the ratio parameter. A similar partition is constructed to the left of $x = 0.7$ with the same parameter value r. Fig. 5.6 compares the solutions computed using the second-order conservative second-order FDM for the Laplacian,

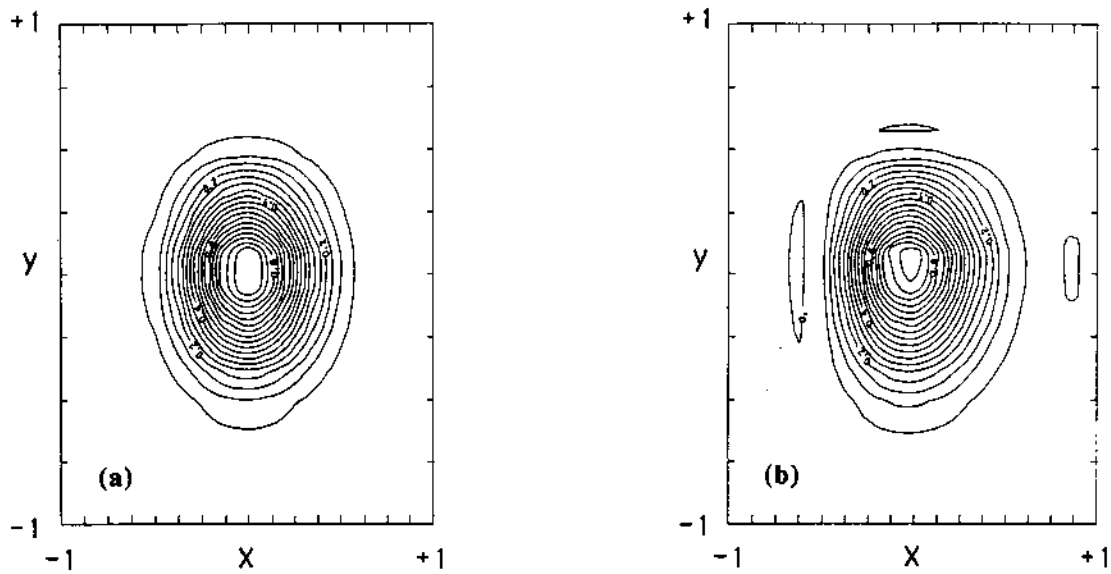

Fig. 5.5. Contour plot of the solution of eq. (5.1) starting with the initial condition and random grid shown in fig. 5.2. The divergence was approximated using the fourth-order centered FVM method [9]. The solution is shown at time $t = 2$ in fig. (a) and at time $t = 8$ in (b).

$$\Delta u_{i,j} \approx \frac{\Delta u_{i+1/2,j}/\Delta x_{i+1/2} - \Delta u_{i-1/2,j}/\Delta x_{i-1/2}}{x_{j+1/2} - x_{i-1/2}} + \frac{\Delta u_{i,j+1/2}/\Delta y_{j+1/2} - \Delta u_{i,j-1/2}/\Delta y_{j-1/2}}{y_{j+1/2} - y_{j-1/2}}, \tag{5.4}$$

with the second-order FVM (4.19).

In fig. 5.7b the considerable distortion of the circular contour lines is evident for the second-order FDM. The contour lines in the second-order FVM solution shown in fig. 5.9c are much more circular. Note that even though the second-order method is an inconsistant approximation to the Laplacian (see fig. 5.6) the solution is still remarkably accurate. This is in agreement with the one-dimensional results of Kreiss et al [11] who showed how, on nonuniform grids, the solutions of the difference equation can converge at a much faster rate to the true solution than a truncation error analyis would suggest. That is, order-of-accuracy analysis in fig. 5.6 is an upperbound on the the convergence rate and, in fact, on nonuniform grids is often a very pessimistic bound. The fourth-order FVM, shown in fig. 5.9d, is considerably more accurate than the second-order method, although the difference is not discernable by eye until later in the calculation. When we compared the methods on random grids similar to the ones used for the wave equation, the errors of the lower order methods tended to cancel out and be much smaller than when the grids were exponentially graded.

6. Summary

In this paper we describe the finite volume method to define differential operators in terms of integrating over finite volumes delineated by the underlying discrete grid. The divergence operator is defined using a discrete version of Stokes' Theorem, the gradient is defined as its dual and the curl and Laplace operators are defined using similar identities. In numerical experiments solving wave and

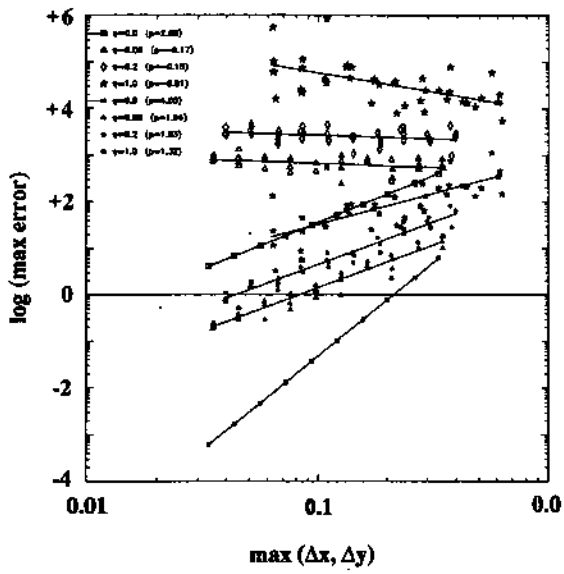

Fig. 5.6. Test of accuracy for the second-order Laplacian approximation on random grids with $\eta = 0.0, 0.5, 0.2$, and 1.0 using the function e^{x+y}. For these grids, the approximate orders (the slope of the least-squares line fit) for the second-order FVM are 2.00, −0.17, −0.15 and −0.81. The corresponding convergence rates for the fourth-order FVM are 4.00, 1.84, 1.83 and 1.32.

diffusion equations on nonuniform grids, we found the fourth-order FVM to be much more accurate than the conservative second-order FDMs and second-order FVM.

Acknowledgements

The authors thank Randy Dougherty, Aric Hagberg, Karla Horsch, and Seymour Parter for their comments and advice. We especially thank Blair Swartz for his many critical insights, advice and patience in helping us understand the intricacies of the FVMs.

Appendix A. Stability of the Laplacian

On a uniform tensor-product grid in the x and y directions with mesh spacings $\Delta x, \Delta y$, and constant mesh ratio $s = \Delta y / \Delta x$, the trapezoidal rule FVM discretization of the Laplacian,

$$-D^2[\bar{\bar{u}}] = -4\overline{\overline{\Delta u}} = (s + s^{-1})(4\bar{\bar{u}}_5 - \bar{\bar{u}}_1 - \bar{\bar{u}}_3 - \bar{\bar{u}}_7 - \bar{\bar{u}}_9) + (s - s^{-1})(\bar{\bar{u}}_4 + \bar{\bar{u}}_6 - \bar{\bar{u}}_2 - \bar{\bar{u}}_8)$$

is a symmetric, conservative, nine-point, $\mathcal{O}(h)$ approximation.

The matrix operator $-D^2$ is also non-negative. We verify this using local mode analysis. Let

$$u(x,y) = -\theta\psi \frac{e^{i\theta x/\Delta x}}{e^{i\theta} - 1} \frac{e^{i\psi y/\Delta y}}{e^{i\psi} - 1}, \text{ so that } \bar{\bar{u}}(x,y) = e^{i\theta x/\Delta x} e^{i\psi y/\Delta y}$$

and define

$$h(\theta,\psi) = -D^2[\bar{\bar{u}}] = 4(s + s^{-1})(1 - \cos\theta\cos\psi) + 2(s - s^{-1})(\cos\theta - \cos\psi)$$

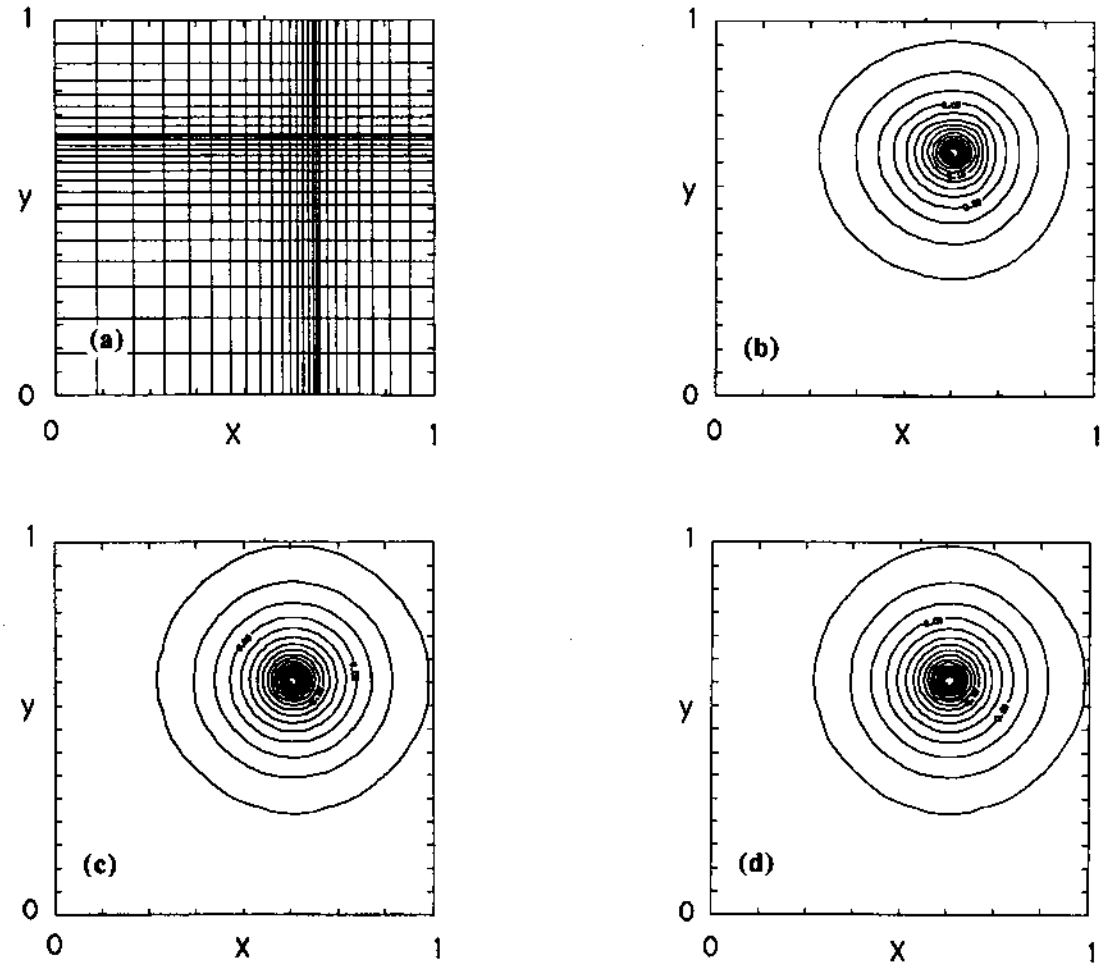

Fig. 5.7. The exponentially graded grid used for the numerical calculations of the diffusion equation (5.2) is shown in (a). (b)–(d) show contour plots of the solution of eq. (5.2) at $t = 0.04$ computed with starting with the initial condition and exponentially graded grid shown in fig. 5.13. In (a), the Laplacian was approximated using the second-order FDM method (5.4). In (c) and (d), the Laplacian was approximated using the second-order (c) and fourth-order (d) FVM method.

if $h(\theta, \psi)$ is non-negative then so is $-D^2$ (see Varga [Var]).

We will show that h is nonnegative at all of its critical points, from which it follows that h is nonnegative everywhere.

The directional derivatives of h are

$$\frac{\partial h}{\partial \theta} = 2\sin\theta\,[2(s+s^{-1})\cos\psi - (s-s^{-1})], \quad \frac{\partial h}{\partial \theta} = 2\sin\psi\,[2(s+s^{-1})\cos\theta + (s-s^{-1})].$$

The critical points of h at which h takes on different values are $(\theta, \psi) = (0,0)$, $(0,\pi)$, $(\pi,0)$, (π,π), and (θ_c, ψ_c), where $\cos\theta_c = (s-s^{-1})/(2(s+s^{-1}))$ and $\cos\psi_c = -(s-s^{-1})/[2(s+s^{-1})]$.

A straightforward calculation shows that

$$h(0,0) = 0, \quad h(0,\pi) = 12s + 4s^{-1} > 0, \quad h(\pi,0) = 4s + 12s^{-1} > 0, \quad h(\pi,\pi) = 0,$$

$$h(\theta_c, \psi_c) = 4(s+s^{-1}) - (s-s^{-1})^2/(s+s^{-1}) > 0.$$

Thus h is non-negative everywhere and the Laplacian approximation is non-negative definite.

We have not been able to prove positive definiteness for the Laplacian when the grid is a tensor product grid with nonuniform spacing. Extensive numerical experiments indicate that it is.

Appendix B. Maximal accuracy

B.1. Discrete gradient approximations

Discrete gradient approximations (∂_x, ∂_y) defined at n points in the plane, $z_i = (x_i, y_i)$, $i = 1, n$, are second-order accurate if for any smooth scalar function f,

$$\partial_x f = \frac{\partial f}{\partial x}\Big|_0 + \mathcal{O}(h^2), \quad \partial_y f = \frac{\partial f}{\partial x}\Big|_0 + \mathcal{O}(h^2). \tag{B.1a,b}$$

For convenience, we have assumed the data has been translated so the gradient is evaluated at the origin. The distance of the points z_i from the origin is measured by h; for example, $h = \sup |z_i|$.

Expanding f in a Taylor series about the origin and defining $f_i = f(z_i)$ $f_0 = f(0,0)$, we have

$$f_i = f_0 + \langle \nabla f_0, z_i \rangle + \langle (Jf)_0 z_i, z_i \rangle + \mathcal{O}(|z_i|^3) \tag{B.2}$$

where

$$Jf = \begin{pmatrix} \partial_x^2 f & \partial_x \partial_y f \\ \partial_y \partial_x f & \partial_y^2 f \end{pmatrix} \tag{B.3}$$

A linear approximation to the directional derivatives can be written as

$$\partial_x f = \sum \alpha_i f_i = \sum \alpha_i \cdot f_0 + \langle \nabla f_0, \sum \alpha_i z_i \rangle + \sum \alpha_i \langle D^2 f z_i, z_i \rangle, \tag{B.4a}$$

$$\partial_y f = \sum \beta_i f_i = \sum \beta_i \cdot f_0 + \langle \nabla f_0, \sum \beta_i z_i \rangle + \sum \beta_i \langle D^2 f z_i, z_i \rangle, \tag{B.4b}$$

Necessary conditions that the approximations be exact for quadratics, which is sufficient to prove the approximation is second order for smooth functions, is that

$$\sum \alpha_i = 0, \quad \sum \alpha_i x_i = 1, \quad \sum \alpha_i y_i = 0, \quad \sum \alpha_i x_i^2 = 0, \quad \sum \alpha_i x_i y_i = 0, \quad \sum \alpha_i y_i^2 = 0, \tag{B.5}$$

where summation is for i between 1 and n.

These conditions can be written as the matrix system

$$A\alpha = b_2 \tag{B.6a}$$

where $b_1 = (0,1,0,0,0,0)^T$, $\alpha = (\alpha_1, \alpha_2, \ldots \alpha_n)^T$, and $(1, x_i, y_i, x_i^2, x_i y_i, y_i^2)^T$ is the ith column of A.

A similar equation is obtained for $\partial_y f$:

$$A\beta = b_2 \tag{B.6b}$$

where $b_2 = (0,0,1,0,0,0)^T$.

Equations (B.5a,b) are solvable if and only if b_1 and b_2 are orthogonal to every solution of the adjoint equation, $A^*\gamma = 0$ where $\gamma = (\gamma_1, \ldots, \gamma_6)$. That is $\langle \gamma, b_1 \rangle = \langle \gamma, b_2 \rangle = 0$.

A solution to $A^*\gamma = 0$ satisfies

$$F_\gamma(x_1, y_1) = \gamma_1 + \gamma_2 x_i + \gamma_3 y_i + \gamma_4 x_i^2 + \gamma_5 x_i y_i + \gamma_6 y_i^2 = 0, \quad i = 1, \cdots, n. \tag{B.7}$$

The solutions to the equation $F\gamma(x,y) = 0$ determine a conic section in the plane. Equation (B.6) requires that all the points (x_i, y_i) must lie on this conic section.

The conditions necessary to solve the adjoint equation, $\langle \gamma, b_1 \rangle = \langle \gamma, b_2 \rangle = 0$, are satisfied when $\gamma_2 = \gamma_3 = 0$ reducing the equation to

$$\gamma_1 + \gamma_4 x^2 + \gamma_5 xy + \gamma_6 y^2 = 0. \tag{B.8}$$

Geometrically this means that the origin, where the gradient is to be approximated, must be the center of the conic section.

When all the data points lie on a conic section determined by (B.6), $F_\gamma(x,y) = 0$, then an analytic interpretation of these results is obtained by considering the function

$$G(x,y) = C + F_\gamma(x,y) \tag{B.9}$$

with gradient

$$(\partial_x G, \partial_y G) = (\gamma_2 + \gamma_5 y + 2\gamma_4 x, \gamma_3 + \gamma_5 x + 2\gamma_6 y). \tag{B.10}$$

Then because $G(z_i) = C$ for $i = 1, n$, and numerical gradient $(D_x G, D_y G) = 0$ is the only consistent value obtainable for the gradient of a function whose value is C at all the data points. This result is correct at the origin where

$$\nabla G = (\gamma_2, \gamma_3)^T = 0, \tag{B.11}$$

requires that $\gamma_2 = \gamma_3 = 0$ which is the solvability condition for (B.6).

Theorem 1. The gradient to a general quadratic scalar function can be computed if and only if:

(a) The points (x_i, y_i) do not lie on a conic section, or

(b) the points (x_i, y_i) lie on conic sections and the point at which the gradient is desired is at the center of all such sections.

B.2. Two argument grids

In numerical calculations often the data points are given on a two-argument logically rectangular grid $(x,y)_{i,j}$. Theorem 1 imposes serious restrictions on the location of nearby grid points when constructing a nine point approximation to the gradient that is exact for quadratics at the central mesh point.

A simple example of a configuration where one cannot compute the gradient of a quadratic function near the grid points is when the points lie on a conic section determined by two intersecting lines and the center point P is at the intersection. This is an undesirable situation since P could easily be far from the grid points z_i if the z_i are on nearly parallel lines. In particular, when $n = 4$, and the four points do not form a parallelogram they lie on a conic section. When they do lie on a parallelogram one can compute the gradient of a quadratic only at the center. When the data points lie on a parabola there is no "center" and no nearby point where the gradient of a quadratic scalar function can be computed exactly.

Another difficulty arises when the grid points are near a conic section. When this happens, the coefficients in the gradient approximation may vary discontinuously as the grid points pass through the conic section. To illustrate this, consider the grid configuration below corresponding to the six points on one side of a nine point stencil:

$$\begin{array}{rccc} (-1+\epsilon_1, 1) & \bullet & \bullet & (1+\epsilon_2,\ 1) \\ (-1,0) & \bullet & \bullet & (1,0) \\ (-1,-1) & \bullet & \bullet & (1,-1) \end{array} \tag{B.12}$$

The six grid points along one side of a nine point stencil often lie nearly along two parallel lines.

Numbering from left to right and top to bottom the matrix A for this stencil is

$$A = \begin{pmatrix} 1 & 1 & 1 & 1 & 1 & 1 \\ 1+\epsilon_1 & 1+\epsilon_2 & -1 & 1 & -1 & 1 \\ 1 & 1 & 0 & 0 & -1 & -1 \\ (-1+\epsilon_1)^2 & (-1+\epsilon_2)^2 & 0 & 0 & 1 & 1 \\ -1+\epsilon_1 & -1+\epsilon_2 & 0 & 0 & 1 & -1 \\ 1 & 1 & 0 & 0 & 1 & 1 \end{pmatrix} \tag{B.13}$$

When $\epsilon_1 = 0$ and $\epsilon_2 \neq 0$, A is invertible and the unique finite difference coefficients for D_y are

$$\begin{array}{rccc} \frac{1}{2} & \bullet & \bullet & 0 \\ -\frac{1}{2} & \bullet & \bullet & +\frac{1}{2} \\ 0 & \bullet & \bullet & -\frac{1}{2} \end{array} \tag{B.14}$$

When $\epsilon_1 = \epsilon_2 = 0$, the matrix A is singular and any convex combination of the two sets of coefficients is permissible.

In general, as a configuration approaches one lying on a parabola, coefficients, (α, β) become unbounded. For, if they remained bound, a convergent subsequence could be found for (α, β) whose limit would provide an approximation exact for quadratics, which is known not to exist.

On a logically rectangular grid (x_i, y_j), if the gradient of a function can be computed to second-order, then the Laplacian of that function can be computed to first order by taking a contour integral of the above gradient. This Laplacian would be symmetric, conservative, consistent with the Laplacian to $\mathcal{O}(h)$, and a nine point approximation.

Thus, the control volume boundary integrals in the FVM approximation of Laplacian of a general quadratic scalar function can be exact (which results in a first-order approximation to the Laplacian

of a smooth function) when the mesh points do not lie on a conic section or the points lie on conic sections, all of which consist of only straight lines and the control volume boundary is at the midpoint line.

If the Laplacian is computed in this fashion and there are grid configurations for which the gradients cannot be approximated to second-order, then it appears that this discretization of the Laplacian will be $\mathcal{O}(1)$ with the possible exception of very special points.

References

[1] M. Abramowitz and I.A. Stegun, eds., Numerical interpolation, differentiation, and integration, Handbook of Mathematical Functions with Formulas, Graphs, and Mathematical Tables 55 (1965) 877–899.
[2] W.G. Bickley, Numerical differentiation formulae for numerical differentiation, Math. Gaz. 25 (1941) 18–27.
[3] W.G. Bickley, Finite difference formulae for the square lattice, Quart. J. Mech. Appl. Math. 16 (1948) 35–42.
[4] L. Collatz, The numerical treatment of differential equations, 3rd ed. (Springer, Berlin, 1960).
[5] P. Collela and P.R. Woodward, The piecewise-parabolic method (PPM) for gas dynamical simulations, J. Comput. Phys. 54 (1984) 174–201.
[6] R.L. Dougherty, A.S. Edelman and J.M. Hyman, Nonnegativity-, monotonicity-, or convexity-preserving cubic and quintic Hermite interpolation, Math. Comput. 52 (1989) 471–494.
[7] S.K. Godunov, A finite difference method for the numerical computation of discontinuous solutions of the equations to fluid dynamics, Mat. Sb. 47 (1959) 271–290.
[8] A. Harten and S. Osher, Uniformly high-order accurate non-oscillatory schemes, I, MRC Technical Summary Report No. kk 2823, May 1985, to appear in SINUM.
[9] J.M. Hyman and B. Larrouturou, The numerical differentiation of discrete functions using polynomial interpolation methods, Appl. Math. Comput. 10/11, pp. 487–506.
[10] J.M. Hyman and J.C. Scovel, Mimetic difference approximations of differential operators, Los Alamos National Laboratory Report (1988).
[11] H.-O. Kreiss, T. Manteuffel, B. Swartz, B. Wendroff and A. White, Supra-convergent schemes on irregular grids, Math. Comput. 47 (1986) 537–554.
[12] J.E. Osborn, The numerical solution of differential equations with rough coefficients, in: Advances in Computer Methods for PDEs-IV, eds. R. Vichnevetsky and R.S. Stapleman (IMACS, New Brunswick, NJ, 1981) pp. 9–13.
[13] G. Strang and G.J. Fix, An Analysis of the Finite Element Method (Prentice Hall, 1973).
[14] B. van Leer, Towards the ultimate conservative difference schemes V. A second-order sequel to Godunovs method, J. Comput. Phys. 32 (1979) 101–136.
[15] R.S. Varga, Matrix Iterative Analysis (Prentice-Hall, 1962).
[16] M. Vinokur, An analysis of finite-difference and finite-volume formulations of conservation laws, J. Comput. Phys. 81 (1989) 1–52.